IOP Publishing | International Atomic Energy Agency Nuclear Fusion

Nucl. Fusion **58** (2018) 016022 (12pp) https://doi.org/10.1088/1741-4326/aa9344

Demonstrating electromagnetic control of free-surface, liquid-metal flows relevant to fusion reactors

M.G. Hvasta[a], E. Kolemen, A.E. Fisher and H. Ji

Princeton University, Princeton, NJ 08544, United States of America

E-mail: MHvasta@princeton.edu

Received 18 January 2017, revised 8 October 2017
Accepted for publication 13 October 2017
Published 13 November 2017

Abstract

Plasma-facing components (PFC's) made from solid materials may not be able to withstand the large heat and particle fluxes that will be produced within next-generation fusion reactors. To address the shortcomings of solid PFC's, a variety of liquid-metal (LM) PFC concepts have been proposed. Many of the suggested LM-PFC designs rely on electromagnetic restraint (Lorentz force) to keep free-surface, liquid-metal flows adhered to the interior surfaces of a fusion reactor. However, there is very little, if any, experimental data demonstrating that free-surface, LM-PFC's can actually be electromagnetically controlled. Therefore, in this study, electrical currents were injected into a free-surface liquid-metal that was flowing through a uniform magnetic field. The resultant Lorentz force generated within the liquid-metal affected the velocity and depth of the flow in a controllable manner that closely matched theoretical predictions. These results show the promise of electromagnetic control for LM-PFC's and suggest that electromagnetic control could be further developed to adjust liquid-metal nozzle output, prevent splashing within a tokamak, and alter heat transfer properties for a wide-range of liquid-metal systems.

Keywords: liquid metal, electromagnetic control, plasma facing components, free-surface flow, galinstan

(Some figures may appear in colour only in the online journal)

1. Introduction and background

Developing plasma-facing components (PFC's) that can withstand the heat and particle fluxes generated by fusion plasmas is an important step towards the creation of an economically viable fusion power reactor. Accordingly, a variety liquid-metal (LM) PFC's have been proposed since the 1970s to address the limitations of solid PFC's made from tungsten, graphite, or molybdenum [1–3]. Compared to solid PFC's, LM-PFC's have the potential to [2, 4–6]:

- provide enhanced power-removal capability
- enable PFC exposure to larger heat-fluxes
- offer a 'self-healing' surface that is unaffected by radiation damage and thermal stresses
- reduce overall system down-time and repair costs
- facilitate tritium production.

Furthermore, several experiments have already shown that using lithium-PFC's on portions of a tokamak interior can greatly improve plasma performance by reducing particle recycling, increasing energy confinement, and suppressing impurity emissions [7–10].

For successful implementation in fusion power reactors, free-surface LM-PFC's (first-walls, limiters, divertors, etc) must accomplish three primary objectives. First, PFC's must be adequately covered with the appropriate thickness of liquid-metal [2, 11]. Second, LM-PFC's must be fast-flowing in order to extract the desired amount of power from the system without becoming too hot. (At elevated temperatures the increased vapor pressure of the liquid-metal can adversely impact plasmas [4, 5, 11].) Lastly, the surface of the LM-PFC

[a] Author to whom any correspondence should be addressed.

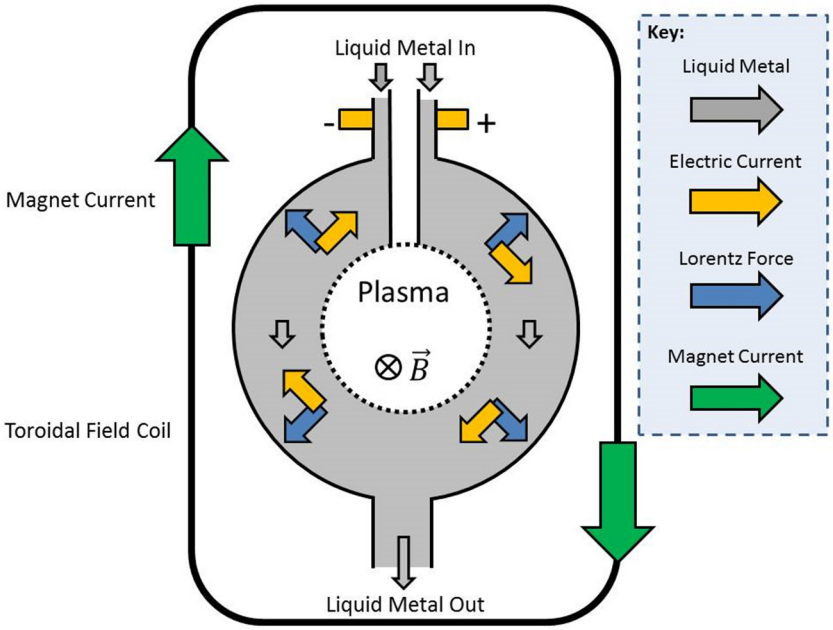

Figure 1. A simple depiction of electromagnetically restrained liquid-metal within a tokamak. Adapted with permission from [13].

must remain smooth under all operating conditions to prevent splashing and avoid 'hot-spots' caused by uneven heating [2, 4, 5, 12].

Various LM-PFC concepts, such as those proposed by Woolley [13, 14] and Zakharov [15, 16], rely on electromagnetic restraint (EMR) to achieve these objectives. To produce EMR during reactor operation, poloidal electrical currents are injected into the flowing liquid-metal. The interaction between the electrical currents and the toroidal magnetic field generates a Lorentz force that presses the liquid-metal against the tokamak walls, as illustrated in figure 1. Due to the low density of lithium (~500 (kg m^{-3}) [17, 18]), only modest current densities are required to generate forces many times stronger than gravity [13], as highlighted by equation (1) and table 1 (As a basis for comparison, the externally applied currents within tokamak toroidal field coils are approximately 3×10^7 (A m^{-2}) [19, 20].)

$$\overbrace{\rho g}^{\text{Gravitational Force}} = \overbrace{jB}^{\text{Lorentz Force}}$$
$$500\ \left(\text{kg m}^{-3}\right)\ 9.8\ \left(\text{m s}^{-2}\right) = j\left(\text{A m}^{-2}\right)\ B\,(\text{T})\,. \qquad (1)$$

Fully-poloidal EMR could be used to promote nearly complete first-wall coverage within a reactor and possibly prevent splashing caused by LM-PFC interactions with the so-called 'plasma wind' [12]. Localized control currents could also be used to adjust nozzle performance [25] or enable smooth flow around complicated geometries or penetrations on the tokamak walls [26].

However, despite the promise of EMR for LM-PFC applications, there is extremely scarce experimental data regarding the electromagnetic control of free-surface, liquid-metal flows. Until now, free-surface liquid-metal research has mostly focused on how different phenomena such as surface waves, heat-transfer, and flow-stability are affected by magnetic fields alone [27–30]. The few papers that have studied the impact of a Lorentz force on free-surface liquid-metals have either not studied flowing systems [31, 32] or have not studied configurations applicable to EMR within tokamaks [33]. For that reason, this paper will present data regarding the electromagnetic control of free-surface, liquid-metal flows relevant to fusion reactors and provide a simple, theoretical framework to explain the findings.

Table 1. The current density within a liquid lithium PFC required to exert a body-force equal to gravity ($g = 9.8$ (m s^{-2})) for various fusion reactors.

Reactor/Ref.	Toroidal magnetic field, B (T)	Approx. current density, j (A m^{-2})
NSTX-U/[21]	1	4900
ITER/[22]	5.3	920
DEMO/[23, 24]	5.86–6	840–820

2. Experiment overview

The liquid metal experiment (LMX), as described by others [34, 35], was designed and built to investigate free-surface, liquid-metal flows and MHD effects relevant to LM-PFC development. During LMX operation, galinstan (see table 2) was pumped through a rectangular, acrylic duct ($w =$ 10.9 (cm), $L \approx 100$ (cm)) with a 0.6 (cm) tall weir at the outlet to maintain a minimum flow height in the channel. The duct was held in the horizontal position, parallel to the floor. A custom Archimedes-style screw pump was used to continuously circulate galinstan throughout the closed-loop system. The galinstan flow rate, $Q = 4$–10 (l min^{-1}), was monitored using a commercially-available Omega Engineering FMG83 electromagnetic flowmeter (see § A.1 for more detail).

As shown in figure 2, flow depth was measured using a laser-sheet diagnostic similar to those used on other open-channel,

Table 2. The properties of galinstan at ~25 (°C) [29, 34, 36–38].

Property	Value	Comments
Density (ρ)	6360–6440 (kg m^{-3})	
Specific heat (c)	295 (J kg^{-1} K^{-1})	
Electrical conductivity (σ)	3.1 × 10^{6} (1 Ω^{-1} m^{-1})	
Surface tension (γ)	0.533 (N m^{-1})	This value is only valid for clean galinstan. It is possible that oxides on the surface can affect surface tension [39].
Kinematic viscosity (ν)	2.98–4 × 10^{-7} (m^{2} s^{-1})	
Composition	Ga = 67.0 wt.%	
	In = 20.5 wt.%	
	Sn = 12.5 wt.%	

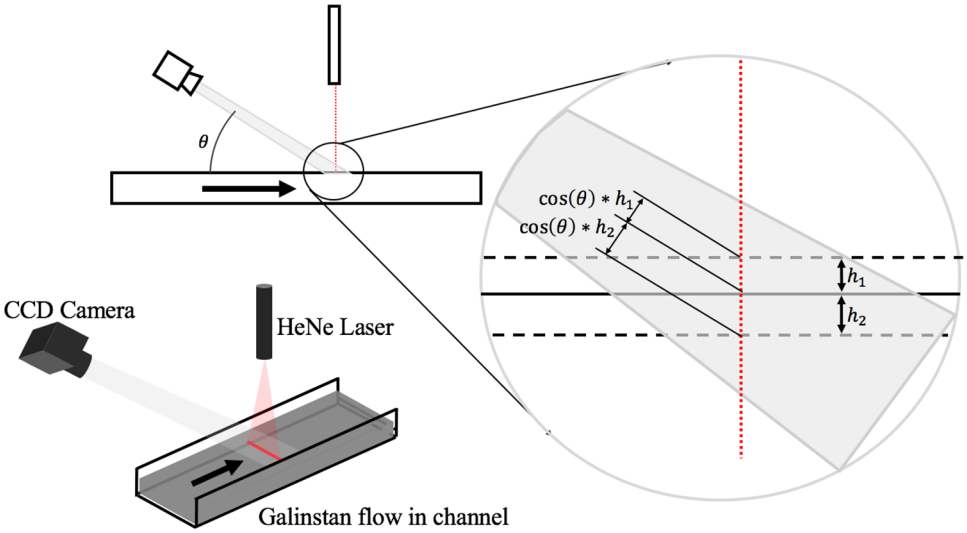

Figure 2. A representation of the laser-sheet height measurement setup used in LMX. In this figure, the variables h_1 and h_2 correspond to arbitrary changes in height from a known reference height.

liquid-metal experiments [40]. The laser-sheet was generated by affixing a cylindrical lens onto a Uniphase 1101P HeNe Laser. All laser sheet videos were taken with a Watec WAT-905H Ultimate CCD camera that was equipped with a ZOOM 7000 Navitar lens. The laser-sheet depth measurements were calibrated by comparing the video data to corresponding height measurements taken using the electrical contact probe method [41, 42]. The electrical contact probe setup used an Aerotech ATS-300 translation stage fitted with a vernier scale yielding 100 (μm) resolution. (See § A.2 for additional calibration data.)

As shown in figure 3, the liquid-metal flowed perpendicular to a magnetic field (B = 0–0.33 (T)) that was generated by an external electromagnet (see § A.3 for more details). Copper electrodes near the inlet and outlet of the channel enabled injected electrical currents (I = 0–140 (A)) to run parallel or antiparallel to the liquid-metal flow. The electrodes were attached to an adjustable AMREL SPS 8-150-000 constant-current power supply. Current density calculations using FEMM [43] and COMSOL indicated that current density was uniform within ~15 (cm) of the electrodes, as shown in figure 4. Since the duct was lined with electrically insulating acrylic, it was assumed that all of the supplied current traveled through the galinstan within the duct during experiments.

During LMX operation small amounts of thermal energy were added to the galinstan by the pump and the ohmic heating produced by the injected electrical currents. (The temperature rise, ΔT, caused by ohmic heating, P_{ohmic}, within the duct was estimated to be ~0.03 (K) using equation (2).) To prevent unwanted temperature increases during long tests, a deionized water—to—galinstan heat exchanger was used to maintain a constant temperature of approximately 25 (°C) throughout the system. The heat exchanger was located between the pump outlet and the channel inlet

$$P_{\text{ohmic}} = \frac{I^2 L}{\sigma h w} = Q \rho c \Delta T. \tag{2}$$

More details regarding LMX setup and operating conditions are given in the appendix. An overview and comparison of LMX operating parameters can be found in table 3.

3. Control of liquid-metal flows using Lorentz force

The equations that govern free-surface, incompressible, liquid-metal flows within LMX can be derived using the following concepts: (1) the conservation of mass, and (2) the momentum-impulse principle. For the rectilinear channel

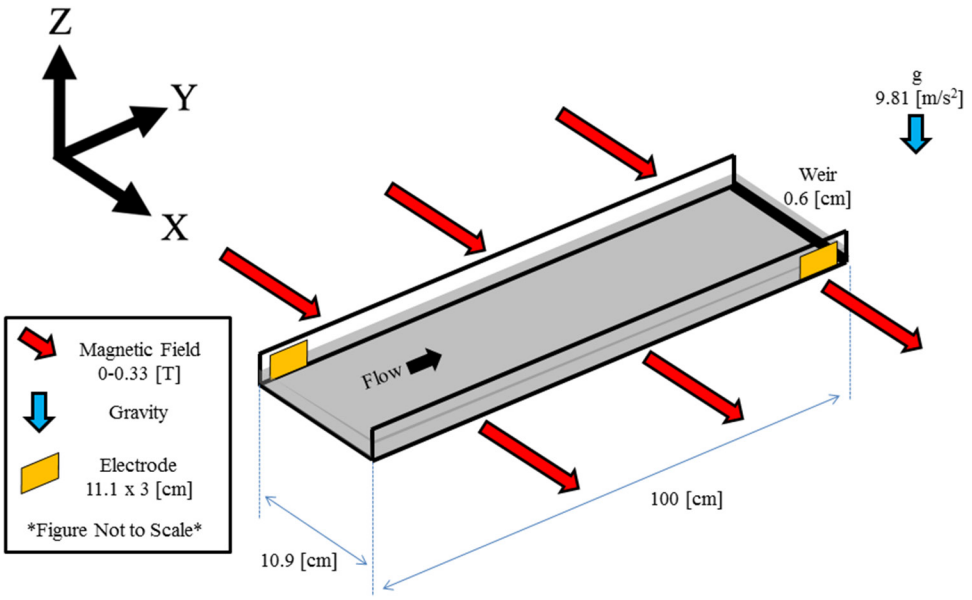

Figure 3. A depiction of the LMX duct. The galinstan flows along the acrylic duct perpendicular to the magnetic field. The electrodes enable electrical currents to run parallel or antiparallel to the liquid-metal flow.

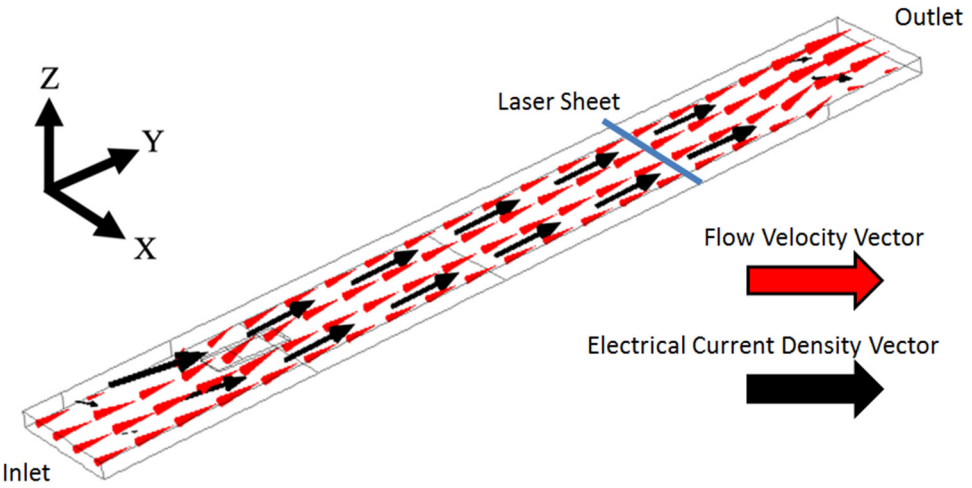

Figure 4. A COMSOL simulation showing the electrical current density vector and the liquid metal flow velocity vector. Both profiles are uniform towards the center of the duct where the height measurements were taken (pump RPM = 1600, $B = 0.3$ (T), $I = 70$ (A)).

Table 3. LMX operating conditions compared to LM-PFC's in other fusion reactors.

Reactor/Ref.	Magnetic field	Current density req. to offset gravity (see equation (1)/table 1)	Interaction parameter	Reynolds #	Liquid metal
Units/definition	B (T)	j (A m^{-2})	$N = \frac{\sigma L B^2}{\rho u}$	Re $= \frac{\rho u L}{\mu}$	
LMX/§ A.3	0.33	14 850	5.3	2.6×10^3	Galinstan
NSTX-U/[21]	1	4900	6.7	$\sim 1 \times 10^5$	Lithium (anticipated)
ITER/[22]	5.3	920	187		
DEMO/[23, 24]	5.86–6	840–820	228–240		

Note 1: LMX flow conditions were approximated as: $u = 0.1$ (m s^{-1}), $L = 1$ (cm).
Note 2: anticipated lithium-PFC parameters are: $u = 10$ (m s^{-1}), $L = 1$ (cm), $T = 400$ (°C).
Note 3: the interaction parameter is the ratio of electromagnetic forces to inertial forces [28, 35].
Note 4: galinstan properties are from table 2. Lithium properties were taken from [17, 18, 44].

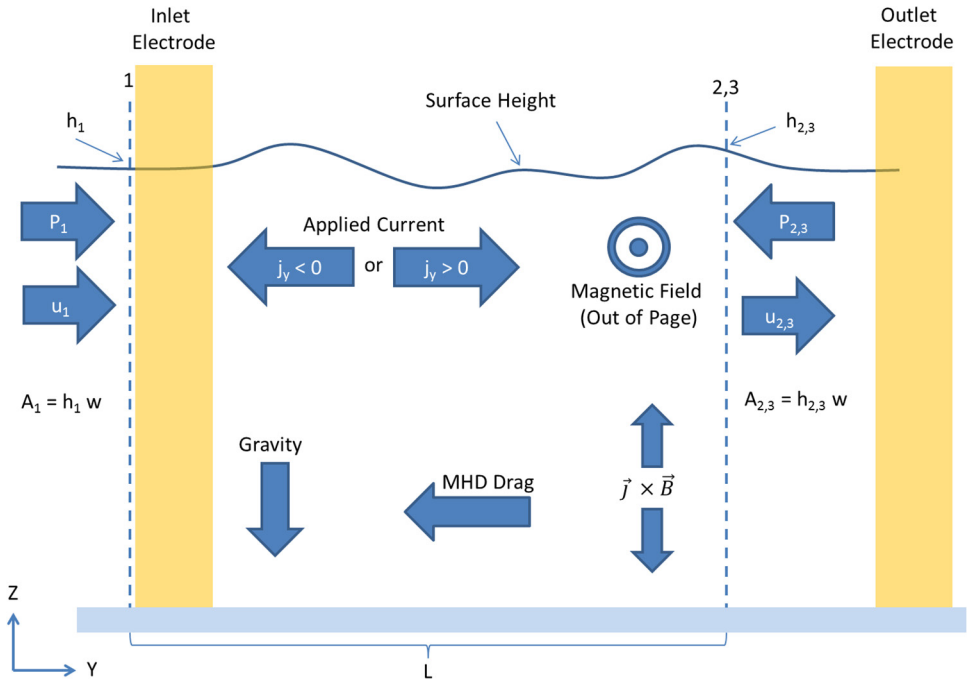

Figure 5. A diagram depicting the pressures and forces acting upon a control volume of flowing metal within LMX. Viscous losses in the system are neglected. The outlet height h_2 corresponds to: $|B_x| > 0$, $|j_y| = 0$. The outlet height h_3 corresponds to: $|B_x| > 0$, $|j_y| > 0$.

used in this experiment, the conservation of mass can be expressed as:

$$\begin{gathered} Q_1 = Q_2 \\ \text{or} \\ wh_1u_1 = wh_2u_2 \end{gathered} \tag{3}$$

where 'Q' is the is the constant volumetric flow rate, 'h' is the height of the liquid, 'u' is the average liquid velocity, and 'w' is the constant width of the duct.

A depiction of the major pressures and forces acting upon the control volume can be found in figure 5. As derived by [45], the sum of the forces acting upon a fluid control volume produces the following change in flow velocity:

$$\sum F = \rho Q\,(u_2 - u_1) \tag{4}$$

where 'ρ' is the density of the fluid.

Neglecting viscous losses, the force balance for a liquid-metal control volume moving across a uniform magnetic without any injected electrical currents can be written as:

$$P_1A_1 - P_2A_2 - \int_0^L P_{\mathrm{MHD}}(y)A(y)\mathrm{d}y = \rho Q\ (u_2 - u_1)\,. \tag{5}$$

As described by [46, 47] the MHD drag on liquid metals flowing within a rectangular geometry with electrically-insulating boundary conditions can be calculated as:

$$\frac{\mathrm{d}P_{\mathrm{MHD}}}{\mathrm{d}y} \approx \frac{\sigma uB^2}{M} \tag{6}$$

when M, the dimensionless Hartmann number, is $\gg$1. For this series of experiments the value of M ranged from about 100–650 (—). The dimensionless Hartmann number, M, is defined as:

$$M = B\,(w/2)\sqrt{\frac{\sigma}{\mu}}. \tag{7}$$

Accordingly, the MHD drag term found in equation (5) can be calculated as:

$$\begin{aligned} \int_0^L P_{\mathrm{MHD}}(y)A(y)\mathrm{d}y &= \int_0^L \frac{\sigma u(y)\,B^2}{M}h(y)w\mathrm{d}y \\ &= \frac{\sigma B^2}{M}\int_0^L u(y)h(y)w\mathrm{d}y. \end{aligned} \tag{8}$$

Since the volumetric flow rate is constant for all points along the duct during steady-state operation (see equation (3)), equation (8) can be rewritten as:

$$\int_0^L P_{\mathrm{MHD}}(y)A(y)\mathrm{d}y = \frac{\sigma B^2}{M}\int_0^L Q\mathrm{d}y = \frac{\sigma B^2QL}{M}. \tag{9}$$

Therefore, equation (5) can be rewritten as:

$$P_1A_1 - P_2A_2 - \frac{\sigma QB^2L}{M} = \rho Q\ (u_2 - u_1)\,. \tag{10}$$

P_1 and P_2 are simply the hydrostatic pressures at average depth so equation (10) can be rewritten as:

$$\left(\frac{\rho gh_1}{2}\right)(h_1w) - \left(\frac{\rho gh_2}{2}\right)(h_2w) - \frac{\sigma QB^2L}{M} = \rho Q\ (u_2 - u_1) \tag{11}$$

or

$$\left(\frac{\rho gh_1^2w}{2}\right) + \frac{\rho Q^2}{h_1w} - \frac{\sigma QB^2L}{M} = \left(\frac{\rho gh_2^2w}{2}\right) + \frac{\rho Q^2}{h_2w}. \tag{12}$$

To build upon this theory, one can also look at tests where externally applied electrical currents run through the liquid-metal

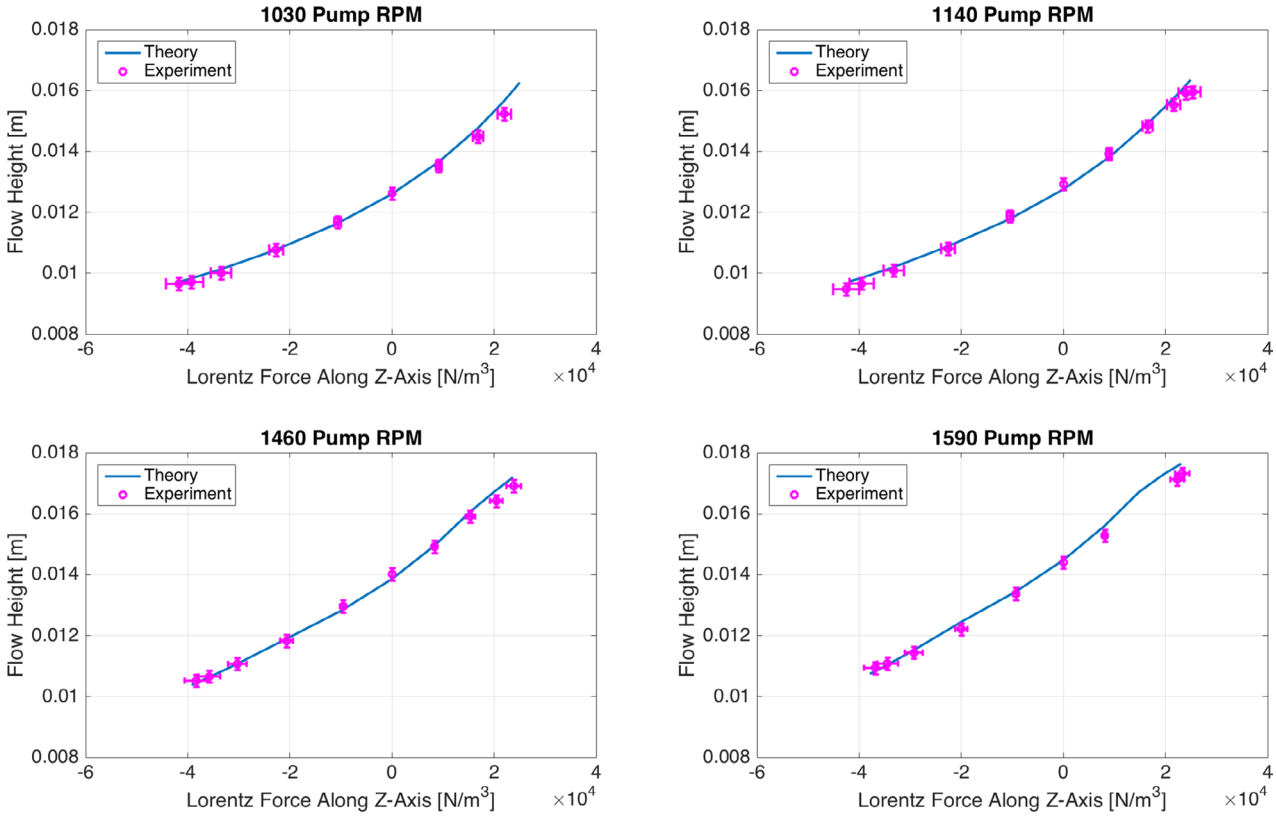

Figure 6. Flow heights of liquid-metal as a function of applied Lorentz force. For this study, $g = 9.80665$ (m s^{-2}), $\rho = 6400$ (kg m^{-3}), $w = 0.109$ (m). (Note: Y-axis error bars correspond to a constant, maximum expected error of ± 200 (μm).)

in the presence of a magnetic field. During this experiment, while the electromagnet was activated and the liquid-metal was flowing through a uniform magnetic field, electrical currents were injected into the flowing liquid metal via the electrodes near the inlet and outlet of the duct (see figures 3 and 5). By adjusting the polarity of the electrodes, LMX could generate a downward (parallel to gravity) or upward (antiparallel to gravity) Lorentz force on the flow. Away from the inlet and outlet, where the current density and magnetic field were largely uniform and the surface waves were negligibly small, the nature of the additional Lorentz body-force acting upon the bulk-flow is analogous to an additional gravitational force [31] that must be accounted for in equation (12). The modified equation for the case when the injected electrical current flows between the electrodes can be re-written as:

$$\left(\frac{\rho g h_1^2 w}{2}\right) + \frac{\rho Q^2}{h_1 w} - \frac{\sigma Q B^2 L}{M} = \left(\frac{\rho g h_3^2 w}{2}\right) + \frac{\rho Q^2}{h_3 w} + \frac{I_y B_x h_3}{2}. \tag{13}$$

Note that, as depicted in figure 5, h_1 is located upstream of the inlet electrode while h_2 and h_3 are located upstream of the outlet electrode. The outlet height h_2 corresponds to: $|B_x| > 0$, $|j_y| = 0$. The outlet height h_3 corresponds to: $|B_x| > 0$, $|j_y| > 0$.

By subtracting equation (12) from equation (13) one finds that the MHD drag terms cancel when the flow rate is held constant and the downstream height is measured at a constant position (L). More specifically, one can determine how applied electrical currents affect the flow height and velocity under constant flow rates and uniform magnetic fields using the following equations:

$$\overbrace{\left(\frac{\rho g h_2^2 w}{2}\right) + \frac{\rho Q^2}{h_2 w}}^{\substack{|B_x|=\text{Constant}>0 \\ |j_y|=0}} = \overbrace{\left(\frac{\rho g h_3^2 w}{2}\right) + \frac{\rho Q^2}{h_3 w} + \frac{I_y B_x h_3}{2}}^{\substack{|B_x|=\text{Constant}>0 \\ |j_y|>0}} \tag{14}$$

or

$$\overbrace{\frac{\rho g h_2^2}{2} + \rho u_2^2 h_2}^{\substack{|B_x|=\text{Constant}>0 \\ |j_y| \,=\, 0}} = \overbrace{\frac{\rho g h_3^2}{2} + \rho u_3^2 h_3 + \frac{j_y B_x h_3^2}{2}}^{\substack{|B_x|=\text{Constant}>0 \\ |j_y|>0}} \tag{15}$$

where

$$j_y = \frac{I_y}{w h_3}. \tag{16}$$

Equations (14) and (15) allow us to compare and predict changes to the liquid-metal flow for two different conditions: (a) with only an applied magnetic field and height measurement at location L (h_2) and (b) with both an applied magnetic field and externally applied current with height measurement at location L (h_3).

For convenience, equations (3), (15) and (16) have been rearranged to yield equation (17). Analytical solutions for h_3 can be readily found using equation (17) and mathematical software, but unfortunately, the exact solutions are too cumbersome to be presented here. Alternatively, the resultant changes in height and velocity due to the added Lorentz forces

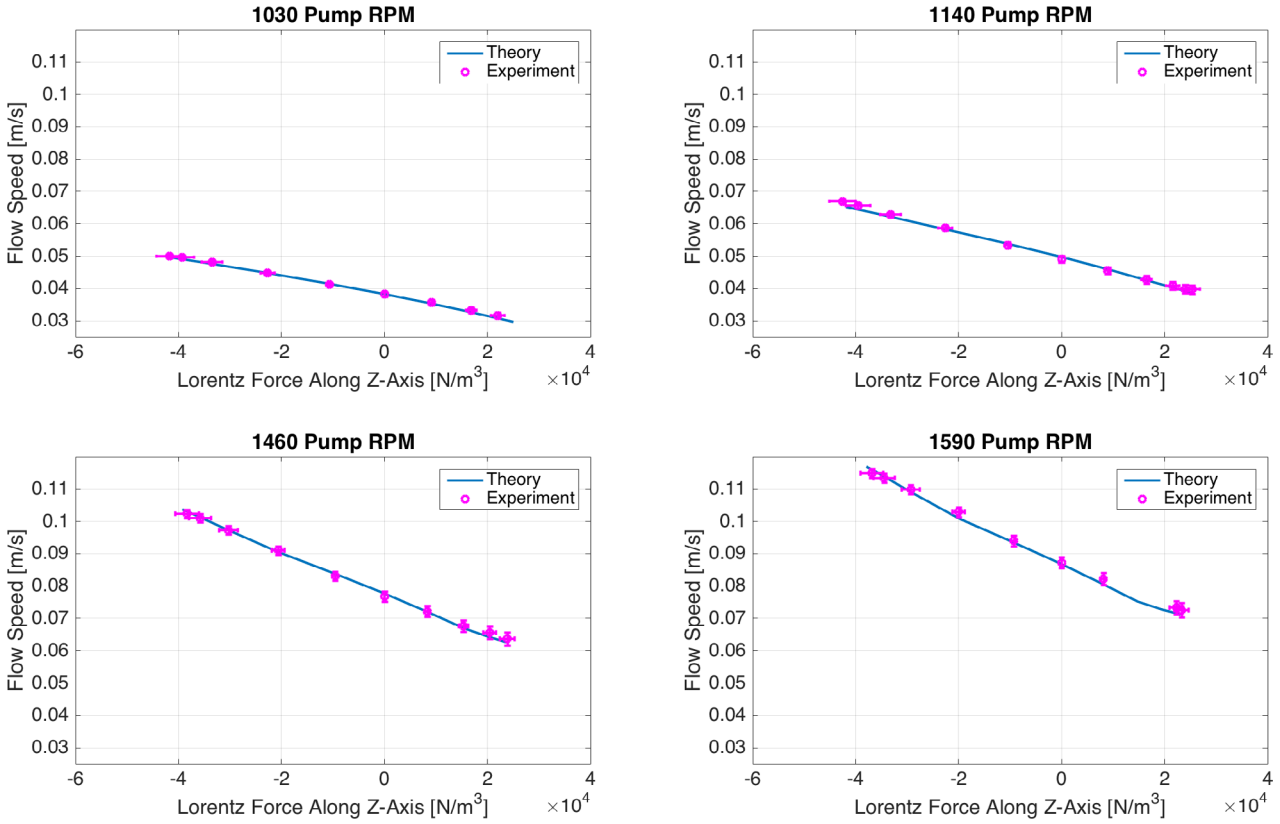

Figure 7. Average flow velocity of liquid-metal as a function of applied Lorentz force. For this study, $g = 9.80665$ (m s^{-2}), $\rho = 6400$ (kg m^{-3}), $w = 0.109$ (m).

can also be calculated by numerically and iteratively solving the equations above and only accepting the real, physically possible solutions (e.g. no negative depths).

$$0 = \left(\frac{\rho g}{2}\right) h_3^3 + \left(\frac{I_y B_x}{2w}\right) h_3^2 - \left(\frac{\rho Q^2}{h_2 w^2} + \frac{\rho g h_2^2}{2}\right) h_3 + \frac{\rho Q^2}{w^2}. \tag{17}$$

Figures 6 and 7 show a comparison of experimentally measured data to theory (equations (15) and (17)). Any abrupt bends in the theory curves are due to flow rate changes at larger magnetic field strength, which are accounted for by K_{Flow} (see § A.1). Since the height measurements were taken at the same location every test, viscous and MHD losses in the system before and after the application of the external current remained effectively constant for a given set of flow conditions.

It may be beneficial to point out that, due to the geometry of the system, Hartmann layers formed along the vertical, non-conducting sidewalls of the channel. For this experiment, where $M \gg 1$, the Hartmann layer thickness (δ) was calculated using equation (18) to be much smaller than the depth ($h \approx 0.01$ (m)) or width ($w \approx 0.1$ (m)) of the liquid-metal flow [48, 49]. The simple model presented to describe LMX flows (equations (12)–(14)) relied on averaged velocity values. Therefore, it is possible that the simple theory worked well for this experiment because the MHD/Hartmann effects flattened the velocity profile within the liquid metal to make it more uniform across the width of the duct [50].

$$M \approx 100 - 650$$
$$\delta = \frac{1}{B\sqrt{\frac{\sigma}{\rho\nu}}} \approx 8.4 \times 10^{-5} - 5.6 \times 10^{-4}\,(\text{m}) \tag{18}$$

4. Discussion of results

The simple theory described in § 3 was able to accurately predict experimental flows within LMX. Hopefully, the given equations will provide LM-PFC designers with a useful approximation of free-surface liquid-metal behavior for future experiments. However, there are several topics that must receive additional consideration to more accurately predict free-surface liquid-metal flows within a fusion reactor.

4.1. Magnetic effects

For this paper the velocity profiles, injected electrical current densities, and magnetic field were all largely uniform. Therefore, calculating the MHD pressure losses was rather straightforward. However, similar calculations for LM-PFC's will most likely be complicated by non-rectilinear flow paths, non-uniform magnetic fields, and electrical current paths through electrically conducting hardware [51, 52]. Nonetheless, in general, MHD pressure-loss scales as [53, 54]:

$$-\nabla P \propto uB^2. \tag{19}$$

So, for larger facilities like NSTX-U or ITER where the toroidal magnetic field could range from approximately 1–6 (T) and flow velocities could be as high as 10 (m s^{-1}), MHD drag on the system is expected to be orders of magnitude larger than what was seen in LMX, as approximated by equation (20)

$$\frac{\nabla P_{\mathrm{ITER}}}{\nabla P_{\mathrm{LMX}}} \sim \frac{u_{\mathrm{ITER}} B^2_{\mathrm{ITER}}}{u_{\mathrm{LMX}} B^2_{\mathrm{LMX}}} \sim \frac{(10)(5.3^2)}{(0.1)\left(0.33^2\right)} \approx 26\,000. \tag{20}$$

4.2. Current density uniformity and electrical boundary conditions

For this experiment, isothermal galinstan flowed through an acrylic duct of uniform width, as described in § 2. Therefore, it was assumed that all the injected electrical current travelled uniformly through the liquid-metal, which greatly simplified analysis [46]. Additionally, FEA modeling showed that the electrical current density within the liquid-metal became uniform a short distance away from the electrodes.

More complex and sophisticated models for fusion reactor LM-PFC's may be needed for four reasons. First, LM-PFC's could be constructed from electrically conductive materials that offer an alternative path for electrical currents. Therefore, not all the injected electrical current will pass through the liquid-metal. Second, LM-PFC's may be formed into complex, non-rectilinear geometries that do not produce uniform electrical current densities. Thirdly, interactions between the liquid-metal and the base-material of the LM-PFC could cause thermoelectric currents to flow within the liquid-metal [32, 55, 56]. Depending on the geometry of the LM-PFC, these thermoelectric currents could complicate the overall distribution of the electrical current density. Lastly, large heat fluxes onto the surface of a LM-PFC could cause steep thermal gradients within the liquid metal [55, 57]. At higher temperatures, the electrical resistivity of candidate liquid metals (Li, LiPb, LiSn, Ga, etc) would be expected to increase [44, 58–60]. Therefore, without thorough thermal mixing, it is possible that more electrical current will travel through the cooler liquid metal closer to the substrate than the hotter, more resistive liquid-metal at the surface of the LM-PFC. Under these conditions the uniform current density assumption used in this paper may not be valid.

4.3. Conservation of mass

The theory described in § 3 assumed that mass is conserved along the liquid-metal flow path. However, this assumption may not apply to all LM-PFC's for several reasons. First, lithium could be ejected from the free-surface flow into the bulk plasma as a result of splashing or sputtering [61]. This ejection of lithium into the plasma could be caused by plasma-PFC interactions or unexpected magnetic transients inducing unwanted Lorentz forces within the liquid-metal.

Second, as previously mentioned, high-temperature operation can cause excessive liquid-metal evaporation [4, 5, 11, 62]. Lithium mass-loss due to evaporation within several full-scale reactor designs is expected to be >10 (l s^{-1}) [63, 64]. The actual evaporative mass-loss rate will depend on a number of factors including the LM-PFC operating temperature, the velocity of the liquid-metal, the duration of the plasma pulse, and the LM-PFC surface area.

Lastly, lithium PFC's can absorb a range of impurities (O, H, H_2O, He, etc) during operation that could cause a noticeable mass-imbalance [65–67]. In many regards this reactive or 'gettering' aspect is a positive aspect of lithium PFC's since impurity levels in the plasma are reduced and plasma recycling is kept low. However, continued or excessive uptake of impurities could change the properties of flowing, free-surface lithium and cause deviations from the theory given in § 3.

To date, most LM-PFC research efforts (CDX-U [8], FLiLi [9], etc) have operated with small amounts of lithium (~1–2 (kg)) so it is possible that even modest levels of impurity could cause noticeable changes to flow and mass-balance of the lithium [8, 9, 68]. Reactor-scale systems will require drastically larger lithium inventories and flow rates of approximately 1.2 (kg s^{-1}) per 1 (MWTh), as shown by equation (21) [18]. Therefore, adsorption of small amounts of impurity may not have a profound impact on larger systems operating over short time-sales. However, over a long enough time, even reactor-scale LM-PFC systems will be susceptible to the accumulation of impurities unless continuously operating, lithium purification systems are developed [69, 70]

$$\begin{aligned} \dot{Q} &= \dot{m} c_p \Delta T \\ 1 \times 10^6\ (\mathrm{W}) &= \dot{m}\left(4169\left(\mathrm{J\,kg^{-1}\cdot K^{-1}}\right)\right)(200\,(\mathrm{K})) \\ \dot{m} &\approx 1.2\left(\mathrm{kg\,s^{-1}}\right). \end{aligned} \tag{21}$$

5. Conclusion and future work

The ability to control the depth and velocity of a flowing liquid-metal within a magnetic field using externally applied electrical currents was demonstrated. The experimental results closely agreed with the simple theoretical framework provided in § 3, which suggests that a similar model could be used to approximate the bulk performance of LM-PFC's within fusion reactors. This model and the EMR technique could also be used to control hydraulic-jumps in LM-PFC's [40], minimize splashing, and offer localized control over heat transfer and temperature profiles of the liquid-metal in particular regions of the reactor interior [57, 71].

Upgrades to LMX are planned to investigate the characteristics of higher flow speeds ($u \approx 2$ (m s^{-1})). Additional diagnostics are currently under development to investigate the impact of Lorentz-force on hydraulic jump phenomena and surface wave properties. Numerical simulations will also be performed to supplement experimental work and possibly

validate other codes that were developed to model free-surface, liquid-metal flows [26].

Acknowledgments

The authors would like to thank E. Gilson, R. Majeski, K. Caspary, M. Modestov, and P. Sloboda for their expertise, assistance, and insights during these experiments. The authors also appreciate the support and essential hardware provided by A. Zwicker.

The research described in this paper was conducted under the Laboratory Directed Research and Development Program (LDRD) at Princeton Plasma Physics Laboratory. This manuscript is based upon work supported by the U.S. Department of Energy, Office of Science, Office of Fusion Energy Sciences, and has been authored by Princeton University under Contract Number DE-AC02-09CH11466 with the U.S. Department of Energy. The publisher, by accepting the article for publication acknowledges, that the United States Government retains a non-exclusive, paid-up, irrevocable, world-wide license to publish or reproduce the published form of this manuscript, or allow others to do so, for United States Government purposes.

The digital data for this paper can be found at: http://arks.princeton.edu/ark:/88435/dsp01x920g025r

Appendix

A.1. Pump and flowmeter

LMX was a closed-loop galinstan system that used a custom Archimedes-style screw pump to circulate galinstan around the system and through the rectangular duct. The pump was powered by a 2 (HP) Leeson DC motor, and pump RPM measured using an Extech 461950 tachometer. Galinstan flow rate was monitored using an Omega Engineering FMG83 electromagnetic flowmeter.

As shown in figure A1, flowmeter measurements for $B = 0$ (T) operating conditions were taken over multiple days to ensure consistency between tests. The EM flowmeter calibration was also verified using an IR-camera particle-tracking technique [42]. For analytical purposes, the output of the pump when $B = 0$ (T) could be accurately described using a linear fit.

The performance of the pump changed when the electromagnet was operating and $B > 0$ (T). As shown in figure A2, for a given RPM the pump flow could change by approximately 15%. This difference is due to MHD drag on the flow [72, 73]. To reliably account for changes in the flow rate a K_{Flow} correction factor was calculated from experimental data, as shown in figure A3 and given in table A1. Using this correction factor, the flow rate during all tests could be accurately calculated using equation (A.1). Externally applied electrical currents did not affect the output of the pump

$$Q = K_{\text{Flow}}\, Q_{B=0}. \tag{A.1}$$

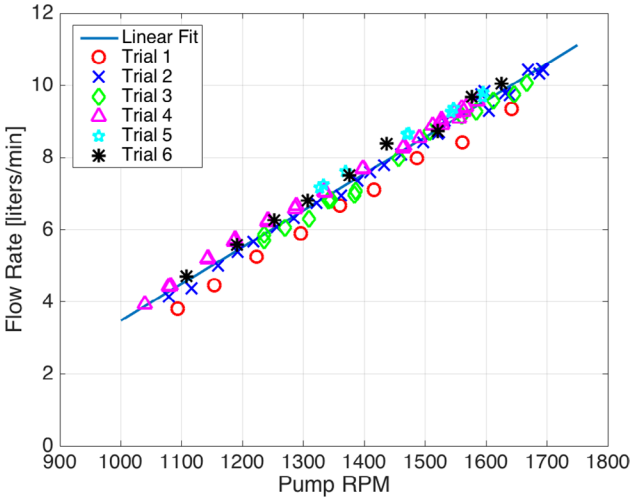

Figure A1. The measured output of the LMX pump with $B = 0$ (T). The pump provided repeatable flow rates over multiple days of testing.

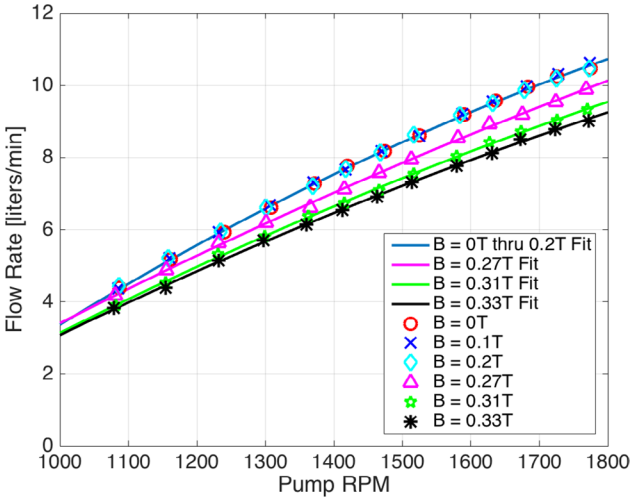

Figure A2. The measured LMX pump performance with magnetic field ranging from 0 to 0.33 (T).

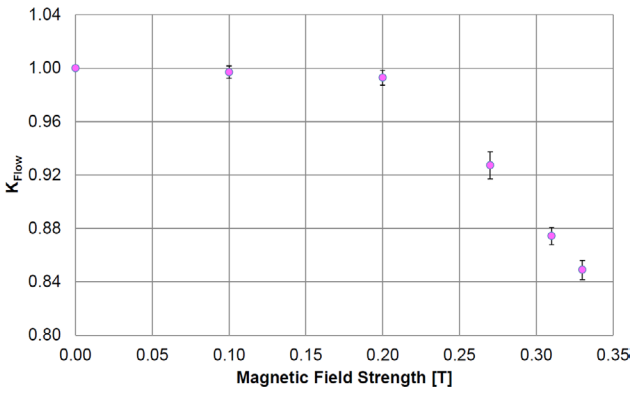

Figure A3. The experimentally determined flow correction factor (K_{Flow}) that accounts for changes in pump performance resulting from MHD drag.

Table A1. The experimentally determined K_{Flow} correction factors.

Electromagnet current (A)	Peak magnetic field (T)	K_{Flow} (—)
0	0	1 (defined)
500	0.1	0.9970 ± 0.0047
1000	0.2	0.9929 ± 0.0056
1500	0.27	0.9272 ± 0.0102
2000	0.31	0.8744 ± 0.0065
2500	0.33	0.8490 ± 0.0072

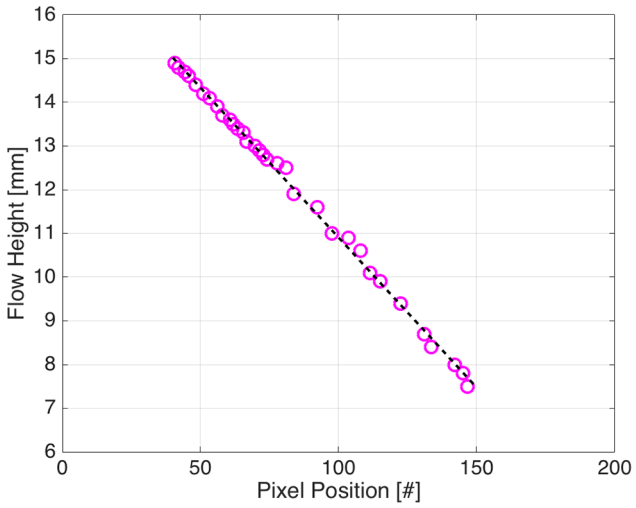

Figure A4. Laser-sheet height calibration data. The points below a height of 12.5 (mm) correspond to galinstan levels that did not spill over the weir. When the depth of the galinstan was greater than 15 (mm) the laser-sheet data was calibrated using the extrapolated linear fit of the data. As detailed in figure 2, the actual height change and the change on the laser-sheet videos scale using a constant coefficient.

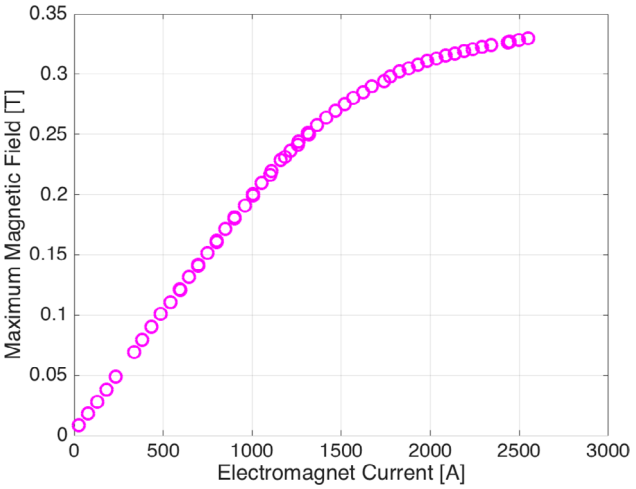

Figure A5. The measured peak output of the electromagnet used in LMX. The cooling system on the magnet did not allow for steady-state operation using larger electromagnet currents.

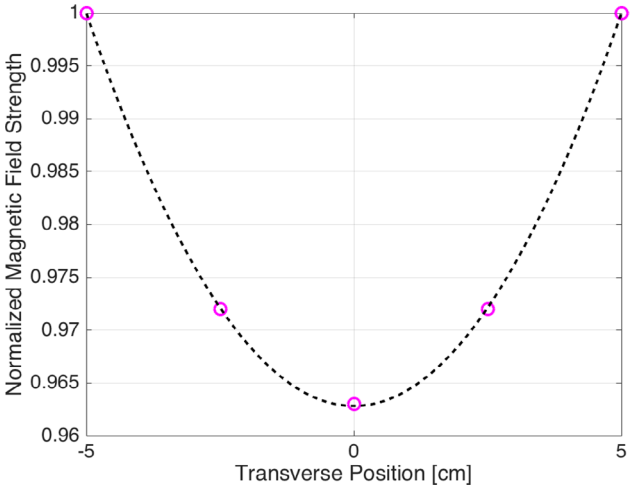

Figure A6. The normalized magnetic field strength across the acrylic channel used in LMX. These data can be represented using a parabolic fit.

A.2. Height measurement calibration

The laser-sheet height measurement technique was calibrated using an electrical contact probe. Results of the laser-sheet depth measurement calibration are given in figure A4.

A.3. Electromagnet performance and field uniformity

The LMX duct was installed horizontally within the air-gap of a C-shaped, water-cooled electromagnet. The electromagnet was approx. 70 (cm) long (in the direction parallel to flow) and provided a magnetic field that was perpendicular to the flow (see figure 3). Before any experiments were performed, the electromagnet output was measured using a LakeShore model 410 gaussmeter, as shown in figure A5. The magnetic field was found to be nearly uniform across the width of the duct, as shown in figure A6.

References

[1] Chrisofilos N.C. 1971 A design for a high power density ASTRON reactor *USAEC Report* UCRL-72957
[2] Abdou M.A. and The APEX Team 1999 Exploring novel high power density concepts for attractive fusion systems *Fusion Eng. Des.* **45** 145–67
[3] Abdou M., Morley N.B., Ying A.Y., Smolentsev S. and Calderoni P. 2005 Overview of fusion blanket R&D in the US over the last decade *Nucl. Eng. Technol.* **37** 401–22
[4] Nygren R.E. *et al* 2004 A fusion reactor design with a liquid first wall and divertor *Fusion Eng. Des.* **72** 181–221
[5] Nygren R.E., Cowgill D.F., Ulrickson M.A., Nelson B.E., Fogarty P.J., Rognlien T.D., Rensink M.E., Hassanein A., Smolentsev S. and Kotschenreuther M. 2004 Design and integration of liquid metal divertors *Fusion Eng. Des.* **72** 223–44

[6] Liao C., Kazimi M.S. and LaBombard B. 1994 MHD effects on liquid metal film flow *Nucl. Eng. Des.* **146** 325–35

[7] Maingi R., Boyle D.P., Canik J.M. and Kaye S.M. 2012 The effect of progressively increasing lithium coatings on plasma discharge characteristics, transport, edge profiles, and ELM stability in the National Spherical Torus Experiment *Nucl. Fusion* **52** 083001

[8] Majeski R. 2004 Testing of liquid lithium in CDX-U *Fusion Eng. Des.* **72** 121–32

[9] Hu J.S., Zuo G.Z., Ren J., Yang Q.X. and Chen Z.X. 2016 First results of the use of a continuously flowing lithium limiter in high performance discharges in the EAST device *Nucl. Fusion* **56** 046011

[10] Ren J., Hu S.U., Zuo G.Z., Sun Z., Li J.G., Ruzic D.N. and Zakharov L.E. 2014 First results of flowing liquid limiter in HT-7 *Phys. Scr.* **2014** 014033

[11] Abdou M. 2001 On the exploration of innovative concepts for fusion chamber technology *Fusion Eng. Des.* **54** 181–247

[12] Morley N.B., Gaizer A.A. and Abdou M.A. 1995 Estimates of the effects of a plasma momentum flux on the free surface of a thin film liquid metal *Fusion Eng. Des.* **28** 176–80

[13] Woolley R. 1997 Electromagnetically restrained lithium blanket *IAEA Workshop on Innovative Approaches to Fusion Energy (Pleasanton, CA)* (www.fusion.ucla.edu/APEX/interim_report/coverfinal.pdf)

[14] Woolley R. 2002 Method and apparatus to produce and maintain a thick, flowing, liquid lithium first wall for toroidal magnetic confinement DT fusion reactors *US Patent* 6,411,666

[15] Zakharov L.E., Gorelenkov N.N., White R.B., Krasheninnikov S.I. and Pereverzev G.V. 2004 Ignited spherical tokamaks and plasma regimes with LiWalls *Fusion Eng. Des.* **72** 149–68

[16] Zakharov L.E. 2003 Magnetic propulsion of intense lithium streams in a tokamak magnetic field *Phys. Rev. Lett.* **90** 045001

[17] Jeppson D.W., Ballif J.L., Yuan W.W. and Chou B.E. 1978 *Lithium Literature Review: Lithium's Properties and Interactions* (Richmand, WA: Hanford Engineering Development Laboratory)

[18] Davison H.W. 1968 *Compilation of Thermophysical Properties of Liquid Lithium* (Washington, DC: NASA)

[19] Yuntao S. and Nishio S. 2005 A consideration on increasing current density in normal conducting toroidal field coil for spherical tokamak power plant *Plasma Sci. Technol.* **7** 2731–3

[20] Kalsi S.S. 1986 Determination of current densities for tokamak superconducting toroidal field coils *Nucl. Eng. Des.* **4** 37–48

[21] Neumeyer C., Avasarala S. and Chrzanowski J. 2009 *National Spherical Torus Experiment (NSTX) Center Stack Upgrade* (Princeton, NJ: Princeton Plasma Physics Laboratory)

[22] US ITER Project Office 2016 WBS 1.1.1.3 toroidal field coil conductor, ORNL 2016-G01409/jpp (Available: www.usiter.org/media/TF.pdf (Accessed: December 2016))

[23] Heller R. 2001 Which superconducting magnets for DEMO and future fusion reactors? *HTS Institute for Technical Physics 4Fusion Conductor—Workshop* (http://itep.kit.edu/hts4fusion2011/downloads/1A4.pdf)

[24] Duchateau J.L., Hertout P. and Johner J. 2007 Discussion about the size of a future fusion demonstration reactor: the impact of the toroidal magnetic field *IEEE Trans. Appl. Supercond.* **17** 1342–7

[25] Tanaka T.J. 2004 Liquid metal integrated test systems (LIMITS) *Fusion Eng. Des.* **72** 83–92

[26] Morely N.B., Smolentsev S., Munipalli R., Ni M.J., Gao D. and Abdou M. 2004 Progress on the modeling of liquid metal, free surface, MHD flows for fusion liquid walls *Fusion Eng. Des.* **7** 3–34

[27] Ying A.Y. *et al* 2004 Exploratory studies of flowing liquid metal divertor options for fusion-relevant magnetic fields in the MTOR facility *Fusion Eng. Des.* **72** 35–62

[28] Rhoads J.R., Edlund E.M. and Ji H. 2014 Effects of magnetic field on the turbulent wake of a cylinder in free-surface magnetohydrodynamic channel flow *J. Fluid Mech.* **742** 446–65

[29] Morley N.B. and Burris J. 2003 The MTOR LM-MHD flow facility, and preliminary experimental investigation of thin layer, liquid metal flow in a 1/*R* toroidal magnetic field *Fusion Sci. Technol.* **44** 74–8

[30] Ji H., Fox W., Pace D. and Rappaport H. 2005 Study of magnetohydrodynamic surface waves in liquid gallium *Phys. Plasmas* **12** 012102

[31] Baker R.C. 1965 Maximum growth rate of Rayleigh–Taylor instabilities due to an electromagnetic force *Nature* **207** 65–6

[32] Mirhoseini S. and Volpe F. 2016 Resistive sensor and electromagnetic actuator for feedback stabilization of liquid metal walls in fusion reactors *Plasma Phys. Control. Fusion* **58** 124005

[33] Alpher R.A., Hurwitz H., Johnson R.H. and White D.R. 1960 Some studies of free-surface mercury magnetohydrodynamics *Rev. Mod. Phys.* **32** 758–69

[34] Nornberg M.D., Ji H., Peterson J.L. and Rhoads J.R. 2008 A liquid metal flume for free surface magnetohydrodynamic experiments *Rev. Sci. Instrum.* **79** 094501

[35] Rhoads J. 2013 *Magnetohydrodynamics and Heat Transfer in a Free-Surface, Flowing Liquid Metal Experiment* (Princeton, NJ: Princeton University Press)

[36] Fisher A.E. 2016 Personal communication with atlantic metals & alloys

[37] Morley N.B., Burris J., Cadwallader L.C. and Nornberg M.D. 2008 GaInSn usage in research laboratory *Rev. Sci. Instrum.* **79** 056107

[38] Hodes M., Zhang R., Wilcoxon R. and Lower N. 2012 On the cooling potential of galinstan-based minichannel heat sinks *13th IEEE ITHERM Conf. (San Diego)* (http://ieeexplore.ieee.org/document/6612637/?reload=true)

[39] Ji H., Fox W., Pace D. and Rappaport H.L. 2005 Study of small-amplitude magnetohydrodynamic surface waves on liquid metal *Phys. Plasmas* **12** 012102

[40] Narula M., Ying A. and Abdou M.A. 2005 A study of liquid metal film flow, under fusion relevant magnetic fields *Fusion Sci. Technol.* **47** 564–8

[41] Slocomb H.W. 1967 Liquid metal level measurement (sodium) state-of-the-art-study, Liquid Metal Engineering Center (https://doi.org/10.2172/4574507)

[42] Hvasta M.G., Kolemen E. and Fisher A. 2017 Application of IR imaging for free-surface velocity measurements in liquid-metal systems *Rev. Sci. Instrum.* **88** 013501

[43] Meeker D.C. Finite element method magnetics, Version 4.0.1 (http://www.femm.info/wiki/FAQ#anchor24 (3 December 2006 Built))

[44] Chi T.C. 1979 Electrical resistivity of alkali elements *J. Phys. Chem. Ref. Data* **8** 340–438

[45] Hickin E.J. 1995 *River geomorphology, International Association of Geomorphologists* (New York: Wiley)

[46] Malang S. and Buhler L. 1994 *MHD Pressure Drop in Duct with Imperfectly Insulating Coatings* (Lemont, IL: Argonne National Laboratory)

[47] Hoffman M.A. and Carlson G.A. 1971 Calculation techniques for estimating the pressure losses for conducting fluid flows in magnetic fields, Lawrence Livermore National Laboratory

[48] Messadek K. and Moreau R. 2004 On the measurement of the Hartmann layer thickness in a high magnetic field *Phys. Fluids* **16** 3243

[49] Krasnov D.S., Zienicke E., Zikanov O., Boeck T. and Thess A. 2004 Numerical study of the instability of the Hartmann layer *J. Fluid Mech.* **504** 183–211

[50] Shercliff J.A. 1953 Steady motion of conducting fluids in pipes under transverse magnetic fields *Math. Proc. Camb. Phil. Soc.* **49** 136–44
[51] Molokov S. and Reed C.B. 2000 Review of free-surface MHD experiments and modeling *Technical Report* ANL/TD/TM99-08 Argonne National Laboratory
[52] Kohnkashbaev I. and Hassanein A. 2002 MHD problems in free liquid surfaces as plasma-facing materials in magnetically confined reactors *Fusion Eng. Des.* **61–2** 223–9
[53] Miyazaki K., Inoue S., Yamaoka N., Horiba T. and Yokomizo K. 1986 Magneto-hydro-dynamic pressure drop of lithium flow in rectangular ducts *Fusion Technol.* **10** 830–6
[54] Morley N.B., Smolentsev S., Barleon L., Kirillov I.R. and Takahashi M. 2000 Liquid magnetohydrodynamics—recent progress and future directions for fusion *Fusion Eng. Des.* **51–2** 701–13
[55] Jaworski M.A., Morley N.B. and Ruzic D.N. 2009 Thermocapillary and thermoelectric effects in liquid lithium plasma facing components *J. Nucl. Mater.* **390–1** 1055–8
[56] Ruzic D.N., Xu W., Andruczyk D. and Jaworski M.A. 2011 Lithium-metal infused trenches (LiMIT) for heat removal in fusion devices *Nucl. Fusion* **51** 102002
[57] Morley N.B. Analysis of thin film liquid metal protection of fusion reactor plasma contact surfaces, UCLA (http://iaea.org/inis/collection/NCLCollectionStore/_Public/23/038/23038165.pdf)
[58] Sobolev V. 2011 Database of thermophysical properties of liquid metal coolants for GEN-IV, Belgian Nuclear Research Centre
[59] Pokorny M. and Astrom H.U. 1976 Temperature dependence of the electrical resistivity of liquid gallium between its freezing point (29.75 °C) and 752 °C *J. Phys. F: Met. Phys.* **6** 559
[60] Pietenpol W.B. and Miley H.A. 1929 Electrical resistivities and temperature coefficients of lead, tin, zinc and bismuth in the solid and liquid states *Phys. Rev.* **34** 1588
[61] Zuo G.Z., Ren J., Ju J.S., Yang Q.X., Li J.G., Zakharov L.E., Ruzic D.N. and HT-7 Team 2014 Liquid lithium surface control and its effect on plasma performance in the HT-7 tokamak *Fusion Eng. Des.* **89** 2845–52
[62] Coenen J.W. 2014 Liquid metals as alternative solution for the power exhaust of future fusion devices: status and perspective *Phys. Scr.* **T159** 014037
[63] Nagayama Y. 2009 *Fusion Eng. Des.* **84** 1380
[64] Tabares F.L. 2016 Present status of liquid metal research for a fusion reactor *Plasma Phys. Control. Fusion* **58** 014014
[65] Ren J., Zuo G.Z., Hu J.S., Sun Z., Li J.G., Zakharov L.E., Ruzic D.N. and Xu W.Y. 2016 Investigations on interactions between the flowing liquid lithium limiters and plasmas *Fusion Eng. Des.* **102** 36–43
[66] Allain J.P., Nieto M., Coventry M.D., Stubbers R. and Ruzic D.N. 2004 Studies of liquid-metal erosion and free surface flowing liquid lithium retention of helium at the University of Illinois *Fusion Eng. Des.* **72** 93–110
[67] Baldwin M.J., Doerner R.P., Luckhardt S.C. and Conn R.W. 2002 Deuterium retention in liquid lithium *Nucl. Fusion* **42** 1318–23
[68] Brooks J.N. 2005 Overview of the ALPS program *Fusion Sci. Technol.* **47** 669–77
[69] Jaworski M.A. 2013 Liquid lithium divertor characteristics and plasma-material interactions in NSTX high performance plasmas *Nucl. Fusion* **53** 083032
[70] Brooks J.N., Baker C.C., Stevens H.C. and Trachsel C.A. 1979 The impurity control system for the STARFIRE commercial fusion reactor *8th Symp. on Engineering Problems of Fusion Research (San Francisco, CA)*
[71] Kirillov I.R., Reed C.B., Barleon L. and Miyazaki K. 1995 Present understanding of MHD and heat transfer phenomena for liquid metal blankets *Fusion Eng. Des.* **27** 553–69
[72] Kandev N., Kagan V. and Daoud A. 2010 Electromagnetic DC pump of liquid aluminium: computer simulation and experimental study *FDMP* **6** 291–318
[73] Baker R.S. and Tessier M.J. 1987 *Handbook of Electromagnetic Pump Technology* (Amsterdam: Elsevier)